Blood oxygen estimation from compressively sensed photoplethysmograph

Conference Paper · October 2010

DOI: 10.1145/1921081.1921084 · Source: DBLP

3 authors, including:

Harinath Garudadri
Qualcomm
129 PUBLICATIONS **1,253** CITATIONS

SEE PROFILE

Blood Oxygen Estimation From Compressively Sensed Photoplethysmograph

Pawan K. Baheti, Harinath Garudadri and Somdeb Majumdar
Qualcomm Incorporated
5775 Morehouse Drive
San Diego, CA, USA, 92121
{pbaheti, hgarudad, smajumda} at qualcomm.com

ABSTRACT

In this work, we consider low power, wearable pulse oximeter sensors for ambulatory, remote vital signs monitoring applications. It is extremely important for such sensors to maintain clinical accuracy and yet provide power savings to enable non-intrusive, long lasting sensors. Our contributions in this work include sub-Nyquist, random sampling of evanescent red and infra red (IR) photoplethysmograph (PPG) signals in real time under the Compressed Sensing (CS) paradigm. We describe the real time platform and demonstrate that the S_pO_2 accuracy is not compromised due to aliasing of ambient light artifacts, even when average number of measurements is much below that of Nyquist rate. We briefly discuss the various modules contributing to overall power consumption of a wireless pulse oximeter sensor and show that 10x reductions in LED power and radio power are possible, without sacrificing the S_pO_2 accuracy.

Categories and Subject Descriptors

C.3 [**Special-purpose and Application-based Systems**]: Real-time and embedded systems; J.3 [**Life and Medical Sciences**]: Medical Information Systems

Keywords

Compressed Sensing, Body Area Networks, Pulse oximeter, Blood oxygenation, Photoplethysmograph, Low power sensors

1. INTRODUCTION

For remote monitoring of vital signs to fulfill its promise, it is extremely important to maintain the clinical accuracy of the measurements. This requires vital signs from the sensors to be free of sensing and motion artifacts; wireless modems to provide a reliable communication link; and the wearable, wireless sensors to be extremely power efficient, so that they can be made small and long lasting. Blood oxygenation (S_pO_2) is considered as one of the most important vital signs and it is typically computed off the data from a pulse oximeter sensor. The benefits of remote monitoring this vital sign in free living conditions, provided that the diagnostic utility is not compromised and the sensor is conducive to non-intrusive monitoring for longer periods has been extensively discussed [1, 2].

Our goal is to address the challenges of maintaining the clinical integrity of data computed from pulse oximeter measurements, including (i) accuracy of S_pO_2, compared to traditional methods, (ii) resilience to motion artifacts, and (iii) integrity of the photoplethysmograph (PPG) morphology, to enable multi-sensory fusion with other vital signs. We consider a decent rule of thumb for the overall power consumption in a wireless pulse oximeter based on commercial, off the shelf components as approximately $1/3^{rd}$ each for (a) LED power for making measurements (b) processing at the sensor node, and (c) modem power for telemetry.

In our previous work [3, 4], we proposed CS based approach to reduce the number of measurements in a pulse oximeter, with validations from off line CS sensing and reconstruction of PPG data (from MIMIC database [5]). The validations included heart rate (HR) and blood pressures (BP) computation from PPG, but did not present validation of S_pO_2 computation from CS measurements, as simultaneous red and infrared PPG waveforms were not available in the MIMIC database. A significant drawback of the works presented in [3, 4] is that the PPG waveforms in the MIMIC database were already low pass filtered. This made the PPG signal essentially sparse, a fundamental assumption for CS to work properly. While [3, 4] showed that HR and BP estimation were not affected by reducing the number of measurements, the effect on S_pO_2 accuracy, specifically due CS sampling of red and infra red PPG waveforms that have not gone through a low pass filter process to make them sparse was not demonstrated.

In this work, we report an experimental S_pO_2 platform, based on Texas Instruments Medical development kit (TI-MDK) [6] to acquire evanescent red and IR (PPG) signals in real time with CS principles. We demonstrate S_pO_2 accuracy in real-time with commercial probes used in pulse oximetry. We modified the software on this device to acquire red and IR PPG in the CS paradigm at at various under sampling ratios (USR). We show that S_pO_2 computation from CS measurements is not affected by aliasing effects of ambient light. This enables us to reduce LED power and radio power by making significantly fewer measurements than required for Nyquist sampling. In section 2, we provide a brief review of CS sensing and reconstruction principles followed by details of the platform, including sensing kernel design for pulse oximeter sensors. We mention alternatives to CS sampling for reducing LED power and discuss potential artifacts due to ambient light and low perfusion conditions. In section 3, we present the performance evaluation of the proposed solution using the TI-MDK platform. In section 4, we consider the overall power requirements from sensing, processing and telemetry perspectives. Power estimates for

Wireless Health '10, October 5–7, 2010, San Diego, USA

sensing and telemetry are presented. Note that processing power required for generic, off the shelf processors may be much higher than that for custom hardware designs. While the algorithms presented here may be adequate for practical solutions in applications such as operating room, sleep staging, etc., motion artifacts present a serious challenge in truly ambulatory situations. The impact of motion artifacts mitigation on accuracy and power budgets for sensing, processing and telemetry in the CS framework is still under investigation and will be discussed in our future work.

2. CS BASED SENSING IN PULSE OXIMETERS

Pulse oximeters use i) red and infrared LEDs, ii) a photodetector and iii) lighting and sampling sequence for LED and photodetector respectively. The modulations in the photodetector output, associated with either of the LEDs is called photoplethysmograph (PPG) and used to estimate S_pO_2, heart rate (HR), etc. Figure 1 illustrates the system flow diagram for PPG sensing. The light from the LED is transmitted/reflected from the tissue and is collected on the photodetector. The ratio of variances from red and IR PPGs is used to estimate oxygen content (S_pO_2) in blood [7]. The lighting sequence for the LED depends upon the desired sampling rate for the PPG signal. Although clinically relevant information in PPG waveforms is typically band-limited to about 10 Hz [8], it is common practice to acquire PPG with sampling rates of 100–250 Hz.

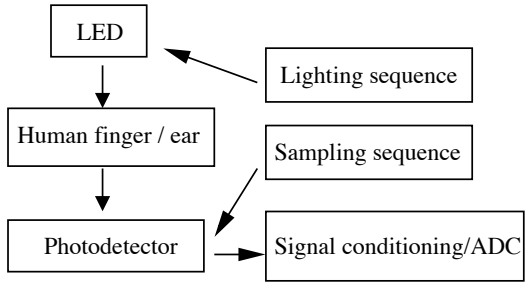

Figure 1: System flow diagram for PPG acquisition.

The LED power in pulse oximeter sensors can be prohibitively large for some BAN applications. The LED power can be reduced by one or more of – (i) lighting the LEDs for shorter duration, (ii) lighting the LEDs with lower intensity and (iii) making fewer measurements by reducing the sampling rate. Rhee et al. make use of faster electronics and reduce the duty cycle of the timing circuit that controls the LEDs, thereby reducing the total time for which LEDs are lit [1]. Tavakolia et al. make use of more sensitive photodiodes and energy efficient transimpedance amplifiers, thereby reducing the intensities at which LEDs are lit [2]. In such approaches, it is important to make sure that adequate SNR is maintained in low perfusion conditions – when there is reduced flow of blood to extremities. It is not possible to reduce the number of measurements, by reducing the Nyquist rate, due to ambient light artifacts. Ambient light can reduce the SNR of the signal received by the photodiodes and can also introduce additional components related power line frequency. The 50/60 Hz artifacts will alias in to the band of interest, if we lower the Nyquist rate below 250 Hz. This can be seen in Fig. 2, with ambient light artifacts at harmonics of power supply frequency (50 Hz in this case).

In low perfusion conditions and high ambient light conditions, it is not always possible to improve the SNR by increasing the LED intensity or the LED duration and integrate the photodiode output for longer durations to improve SNR. This is because ISO specifications [9] limit the maximum power delivered to the LEDs such that the temperature at the probe does not exceed 41^oC, when the skin temperature is initially at 35^oC. If it is necessary to increase the LED power beyond this, special modes on the device are required and an operator shall administer the pulse oximeter. In such special modes, the application times shall be limited 4 hours continuous operation for 43^oC and 8 hours for 42^oC.

Our previous work presented an approach to reduce the number of measurements based on CS [3, 4] and we present S_pO_2 validation here. It will become evident that this approach overcomes many of the ambient light artifact challenges discussed above. Further, it may be possible to increase the LED power in low perfusion conditions, as we reduce the number of measurements compared with Nyquist sampling. Note that the approach of using CS sampling is complimentary to reducing duration and/or intensity of LEDs and it is possible to use a combination of approaches to reduce LED power, without compromising the clinical uses of pulse oximeter sensors.

2.1 CS Overview

In this section, we briefly review the CS approach. Consider a short term segment of a PPG signal, denoted by $N-$dimensional vector $\mathbf{x}$ where f_s is the Nyquist sampling frequency of $\mathbf{x}$. Let matrix $\mathbf{W}$ be some basis functions, consisting of $N\times N$ elements. Given our familiarity with spectral domain, we consider $\mathbf{W}$ as Gabor functions, consisting of various cosine waves with time support limited by Gaussian window functions at different scales, such that the (i,j) entry of $\mathbf{W}$ is given by

$$[\mathbf{W}]_{i,j} = \cos\left(\frac{2\pi(i-1)(j-1)}{2N}\right) \times \exp\left(-\frac{(i-1)^2(j-N/2)^2}{wN^2}\right). \quad (1)$$

The term w is associated with the width of the Gaussian kernel in the Gabor basis. We normalize each row of the matrix $\mathbf{W}$ such that the corresponding L_2-norm is equal to 1. The transform domain representation of PPG signal $\mathbf{y}$ can be computed as

$$\mathbf{y} = \mathbf{W}\mathbf{x}. \quad (2)$$

If $\mathbf{x}$ has a lot of redundancy in the time domain, then there are only M components with magnitude greater than ϵ in $\mathbf{y}$, where $\epsilon \ll \max(\mathbf{y})$, and $M \ll N$. In this case, we call $\mathbf{W}$ a sparse basis. In the CS paradigm, if one is able to construct a measurement matrix $\mathbf{H}$ of dimension $K\times N$ that is statistically incoherent with the sparse basis $\mathbf{W}$, then only K measurements given by

$$\mathbf{r} = \mathbf{H}\mathbf{x}. \quad (3)$$

are adequate to estimate $\mathbf{y}$ with a high probability of some small reconstruction error, provided $K \geq M \log N/M$[10, 11]. One approach to signal reconstruction from $(\mathbf{r}, \mathbf{H}, \mathbf{W})$ is an iterative process called the gradient-projection based sparse reconstruction (GPSR) [12], given as

$$\hat{\mathbf{y}} = \min_{\mathbf{y}} \left[\|\mathbf{H}\mathbf{W}^{-1}\mathbf{y} - \mathbf{r}\|^2 + \tau \sum_{i=1}^{N} |[\mathbf{f}]_i[\mathbf{y}]_i| \right] \quad (4)$$

$$\text{and } \hat{\mathbf{x}} = \mathbf{W}^{-1}\hat{\mathbf{y}}. \quad (5)$$

In the optimization process of Eq. 4, the first term enforces measurement fidelity and the second term enforces signal sparsity. The quantity τ is a non-negative parameter providing relative weight of L_2-norm and L_1-norm in the cost function. The terms $[\mathbf{f}]_i$ and $[\mathbf{y}]_i$ denote the i^{th} element of vectors $\mathbf{f}$ and $\mathbf{y}$, respectively. The term

$\mathbf{f}$ was introduced to incorporate *a priori* sparsity information in the L_1-norm during reconstruction in [4], and it is typically computed off line. The vector $\mathbf{f}$ in Eq. (4) enforces the low-pass nature of PPG signal and avoids the estimation of high-frequency artifacts during the CS reconstruction.

2.2 Sensing Kernel for PPG

We now describe the sensing process for acquiring PPG signals. It can be seen from Fig. 2 that red and IR PPG signals are indeed sparse in the spectral domain, with most components of interest below 10 Hz and ambient light artifacts at harmonics of power line frequency. Recall that the CS framework requires a measurement matrix $\mathbf{H}$ that it is statistically incoherent with the sparse basis $\mathbf{W}$. The time-frequency structure of PPG signals as shown in figure 2 suggests sampling the signal at random locations in time and reconstructing in frequency (e.g. sparse basis $\mathbf{B}$), as shown in Eq. 4. We refer to the reconstruction obtained from this process as CS-PPG. Let $\mathbf{P}$ denote a $K-$dimensional vector containing unique entries (chosen at random) with each element bounded between 1 and N. This essentially provides the K random locations to select the elements from $\mathbf{x}$. $\mathbf{H}$ can be mathematically represented as a matrix of dimension $K \times N$, where every i^{th} row is an all-zero vector with 1 at the location given by the i^{th} element of $\mathbf{P}$. Since we wish to make fewer measurements than N in order to reduce sensing power, we choose $K < N$ and define under-sampling ratio (USR) as N/K. In practice, the sensing can be implemented by incorporating an "enabling" functionality in the circuitry that control LEDs and the photodetector, at time instances corresponding to the locations in $\mathbf{P}$. Note that for traditional Nyquist sampling systems, the sample and hold (S/H) and quantization for analog-to-digital conversion (ADC) is driven by interrupts occurring at uniform intervals in time, corresponding to the Nyquist rate. In order to implement the CS based random sampling in a real-time environment, the interrupt generation logic can be modified to generate the next sampling instance as specified by $\mathbf{P}$. Let f_{clock} be the clock frequency associated with the system and f_s is the desired Nyquist sampling frequency. We define MINDUR as f_{clock}/f_s: the minimum duration in number of system ticks, between two Nyquist samples. In the CS framework the interrupt duration between the $(i-1)^{th}$ and i^{th} sampling instances is then given by

$$\mathbf{\Delta}_i = (\text{MINDUR}) \cdot (\text{USR}) + J(i), \tag{6}$$

where $J(i)$ is a random jitter introduced for i^{th} sample and $J(i) \leq$ MINDUR, $\forall i$. In this work, we used a Linear Feedback Shift Register (LFSR) [13] counter to generate $J(i)$. We assume that the LFSR seed is synchronized between the sensor and the receiver periodically, via some out-of-band signaling scheme.

2.3 CS Reconstruction for PPG

For CS reconstruction as shown in Eq. 4, one can incorporate the sparsity prior in the term $\mathbf{f}$. Consider the case when the ambient signal is modeled as sinusoid of frequency $f_{ambient}$ Hz (for example, $50/60$ Hz). The ambient artifact is typically removed by making an independent measurement of the ambient light via electronic multiplexing techniques (i.e., making an ambient measurement followed by red PPG measurement, and so on.) [14]. Here, the finite switching time for the electronic multiplexing still introduces high frequency components in the PPG, requiring higher Nyquist rate to avoid aliasing. Consider the subtraction of a large signal $x_{ambient}(t)$ from a signal $x_{ppg}(t+T_s) + x_{ambient}(t+T_s)$ where $T_s (i.e., 1/f_s)$ is the sampling period, then the resulting ambient-free PPG signal will still contain the residual error proportional to derivative of the ambient noise. It is therefore very critical to acquire the PPG signal at $2 \cdot f_{ambient}$ Hz, to avoid the aliasing effects during Nyquist sampling. Since the PPG signal can still be very sparse, the number of samples/second for CS acquisition can be much lower than that for Nyquist acquisition and still be resilient to ambient light artifacts.

2.4 Implementation

In this section, we describe the implementation of above on a Texas Instruments Medical Development Kit (TI-MDK) [6]. Our complete implementation consists of the following components: (i) Oxilink finger probe, (ii) TI's MDK pulse oximeter front end, (iii) C5505 DSP from TI MDK, (iv) Embedded software application on MDK for Nyquist and CS sampling, (v) Bluetooth communication module (Ezurio) (vi) PC side reconstruction routines and (vii) Real-time display of the PPG waveforms. The Finger probe has a photo detector and two LED's, one red and infrared, to transmit light across the fingertip. The probe is connected to the front end board through a DB9 connector. The initialization of the hardware is done by the C5505 DSP. The C5505 reads the digitized infrared and red signals from SpO2 front end board and amplifies the same. The amplified signal is provided to PC application over the bluetooth interface for processing and display. The Nyquist sampling is performed at $f_s = 250$ Hz to overcome first two harmonics of power line frequency, and the CS-PPG sampling was done for USR values of 5, 10 and 15. The clock frequency for the TI MDK is 50 MHz. The interrupts to light up the red and infrared LEDs at random intervals was based on the interrupt definition given in Eq. (6). This platform allows us to validate CS based PPG sensing and reconstruction in addition to evaluate accuracy of SpO2 computation.

3. PERFORMANCE EVALUATION

In [3, 4], extensive set of simulations evaluating the reconstruction and heart rate estimation performance based on CS-PPG were reported, but did not include S_pO_2 validation. In this work our goal is to present validation of S_pO_2 estimation and address the challenges associated with ambient light artifacts due to sub-Nyquist sampling.

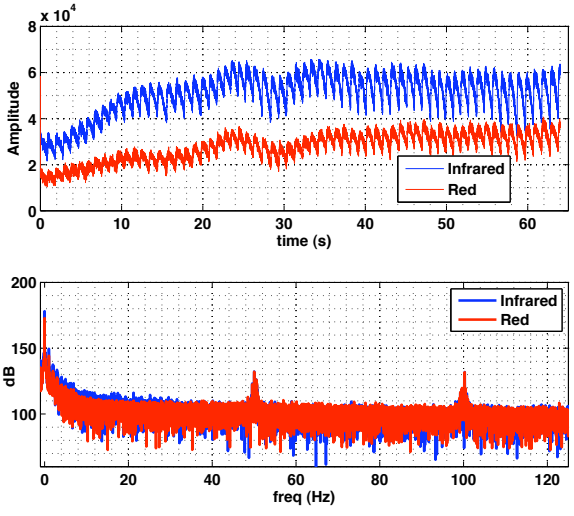

Figure 2: *Top figure*:Snapshot of the red and infrared PPG signals, *Bottom figure*: Fourier transform of the signals from above. The power line frequency in this case was 50 Hz. Contributions due to ambient light artifacts can be seen around 50 Hz and 100 Hz.

Referring to Figure 2, the effect of ambient light on S_pO_2 estimation can be easily appreciated. Figure 2 shows the waveforms and spectra of red and infrared PPG segments acquired at Nyquist sampling rate of 250 Hz, with ambient light artifacts at power line harmonics. Note that the useful noise-free PPG spectral content is typically bandlimited up to 10 Hz [8]. Because the PPG signal is discretely acquired, it is not possible to apply the anti-aliasing filter without acquiring the signal at high sampling rate (greater than 200 Hz typically). If the sampling rate is chosen to be smaller than 120 Hz when ambient light artifact is present, then this would result in aliasing effects as discussed in the previous section. Here we demonstrate that aliasing-free PPG waveforms can be reconstructed from CS-PPG samples at average sampling rates of lower than 50 Hz. Figure 3 demonstrates this in a qualitative manner.

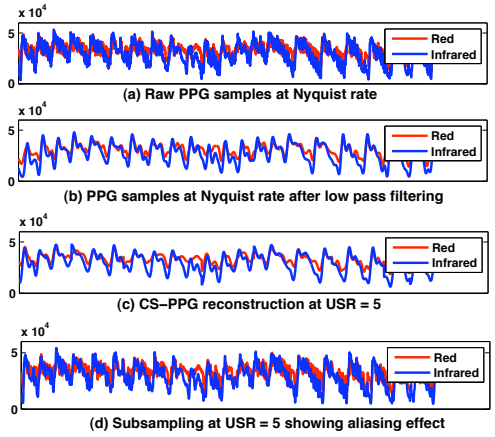

Figure 3: Effect of ambient light artifacts and PPG sampling frequency. (a) Raw PPG samples from the photodetector, sampled at 250Hz. (b) PPG waveforms with 20Hz low pass filter to remove power line frequency components due to ambient light. (c) CS-PPG reconstruction for average sampling rate of 50 samples/second (corresponding to USR=5). (d) Effect of aliasing with Nyquist sampling at 50 samples/second.

Figures 3(a) and 3(b) show the raw and low pass filtered versions of PPG. Figure 3(c) has same number of measurements as in Figure 3(d); but do not have the aliasing components due to ambient light, as they have been suppressed via the regularizing parameter $\mathbf{f}$ in the reconstruction process defined by Eq. (4). Figure 3(d) shows that simply lowering the Nyquist sampling rate to f_s/USR will not work, as it is not possible to low pass filter the PPG data prior to S/H and quantization. In the current implementation, we used the S_pO_2 estimation algorithm described in [6]. In [6], S_pO_2 computation is based on PPG data over three heart beats, but used a fixed window of 2 seconds. We remove the dc bias and compute root-mean-square (RMS) values for both infrared and red signals over this window. The ratio of red and infrared RMS values is compared with a table look-up to obtain the S_pO_2 values [6]. Figure 4 shows the S_pO_2 waveforms for different PPG acquisition schemes and Figure 5 shows the mean and standard deviation values averaged over 60 seconds. These results are for one subject, with CS samples obtained by randomly sampling Nyquist data for fair comparison. In order to validate CS samples directly, as shown by Eq. 6, we made the measurements of the CS-PPG samples (USR = 10) and Nyquist PPG samples ($f_s = 250$ Hz) one after the other (with no time gap and same finger position). The heart rate as inferred from both the cases was roughly the same and varied from 70 to 72 BPM. Figures 6(a) and 6(b) show the low-pass-filtered Nyquist PPG data and CS-PPG waveforms, respectively. Figures 6(c) shows the S_pO_2 estimated from the above. While further validations are still needed, the results presented so far clearly demonstrate that number of measurements can be reduced without being susceptible to ambient light artifacts – resulting in substantial savings in sensing power for pulse oximeters.

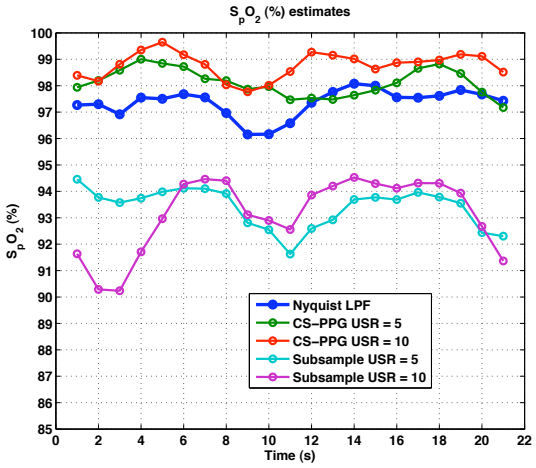

Figure 4: S_pO_2 estimation with PPG acquired at Nyquist rates of 250, 50 and 25 samples/second; and CS-PPG acquired at average sampling rates of 50 and 25 samples/second, corresponding to USR=5 and 10, respectively.

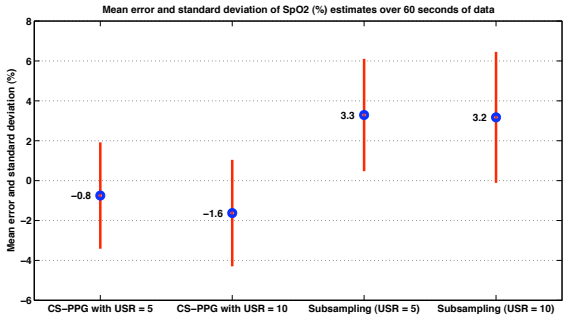

Figure 5: Mean and standard deviation of S_pO_2 estimation with PPG acquired at Nyquist rates of, 50 and 25 samples/second; and CS-PPG acquired at average sampling rates of 50 and 25 samples/second, corresponding to USR=5 and 10, respectively. Nyquist PPG acquisition at 250 samples/second is assumed to be the ground truth.

4. SENSOR POWER REQUIREMENTS

In this section we present rough estimates for the predicted sensor power consumption. We use some baseline estimates for the BT radio, LED drive currents and TI-MDK processor to compute the power. We note that the maximum current drawn by the DSP core is $140mA@3.3V$. The processor time consumed is divided into two tasks: (i) ISR measured to be 600μsec per sample and (ii) data communication theoretically estimated to be 400μsec per sample. Therefore energy consumed by the processor per sample $= 3.3 \times (140 \times 10^{-3}) \times ((600+400) \times 10^{-6}) = 0.5mJ$. For the finger Probe LEDs, the maximum current drawn is $80mA@3.3V$.

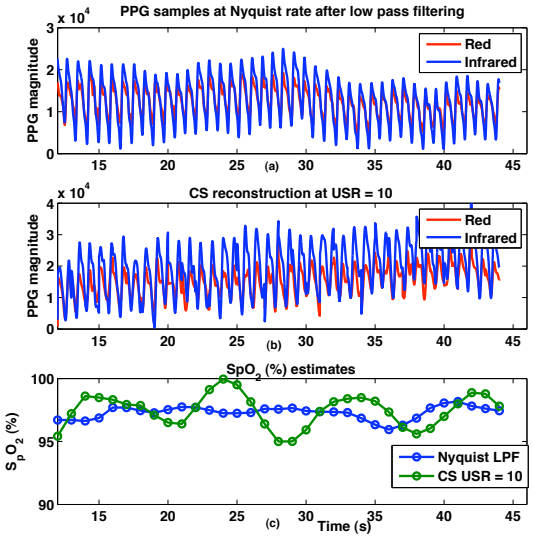

Figure 6: Experimental validation of the S_pO_2 estimation from CS-PPG data acquired at USR = 10.

The "ON" time for both red and infrared LEDs is equal to 50μsec. Therefore energy consumed by the LEDs per sample $= 3.3 \times (80 \times 10^{-3}) \times ((50+50) \times 10^{-6}) = 0.03mJ$. For Bluetooth communication the typical current drawn is $36mA@5V$. The BT baud rate is set to $= 115200bps = 14400bytes/sec$. The time taken for sending one sample (infrared and red, comprising 4 bytes) is $= 4/14400sec = 0.27msec$, Therefore Bluetooth energy consumption per sample $= 5 \times (36 \times 10^{-3}) \times (0.35 \times 10^{-3}) = 0.05mJ$.

The power can be calculated by adding all the three components above and multiply by number of samples per second. For Nyquist acquisition the total power consumption is given by $= (0.5mJ + .03mJ + .05mJ) \times f_s$ which equals to 145 mW for $f_s = 250Hz$. Similarly the power consumption for CS-PPG acquisition is given by $0.6 \cdot f_s/\text{USR}mW$, resulting in $14.5mW$. It should be noted that the C5505 DSP is generic processor, to facilitate developing medical devices and not an optimal for real deployments. The processing required for estimating can be easily accomplished with an order of magnitude lower power than that with C5505. Further, motion artifacts mitigation may change sensing, processing and radio power budgets.

5. CONCLUSIONS

Most BAN applications for healthcare require ultra low power sensing and need to maintain functional integrity of the signals in the presence of sensing artifacts, packet losses, etc. For pulse oximeter sensors, the LED power can be prohibitively large. We discussed various approaches to reduce the LED power and identified the potential ambient light artifacts arising from such optimizations. We described a CS based approach to reduce the LED power and presented S_pO_2 validation including details of implementation. We showed that the proposed approach does not have the ambient light artifacts and is complimentary with other approaches for further power reduction. We presented examples of S_pO_2 estimation using 10x fewer samples than Nyquist-rate sampled PPG. The proposed approach has the additional benefit of reducing the number of samples sent over the air, resulting in lower modem power. We presented power estimates for sensing and telemetry with the proposed approach.

For any clinical device such as a pulse oximeter, extensive clinical studies and validation are required. As the signal prior $\mathbf{f}$ used for PPG reconstruction in Eq. 5 is very weak, in the sense, it just enforces the low-pass nature of PPG signal, it should hold for most clinical usage scenarios. A rigorous validation requires prototype devices, regulatory approvals for clinical trials, clinicians, human subjects, etc. and such a clinical study is beyond the scope of the current work.

6. REFERENCES

[1] S. Rhee, B. Yang, and H. H. Asada. Artifact-resistant power-efficient design of finger-ring plethysmographic sensors. *IEEE Transactions on Biomedical Engineering*, 48:795–805, July 2001.

[2] M. Tavakolia, L. Turicchia, and R. Sarpeshkar. An ultra-low-power pulse oximeter implemented with an energy-efficient transimpedance amplifier. *IEEE Transactions on Biomedical Circuits and Systems*, 4:27–38, Feb 2010.

[3] P. K. Baheti and H. Garudadri. Heart rate and blood pressure estimation from compressively sensed photoplethysmograph. In *BodyNets 2009 conference*, April 2009.

[4] P. K. Baheti and H. Garudadri. An ultra low power pulse oximeter sensor based on compressed sensing. In *Wearable and Implantable Body Sensor Networks, 2009. BSN 2009. Sixth International Workshop on*, pages 144–148, June 2009.

[5] G. B. Moody and R. G. Mark. A database to support development and evaluation of intelligent intensive care monitoring. In *Proc. Computers in Cardiology*, pages 657–660, Indianapolis, IN, September 1996.

[6] http://focus.ti.com/lit/an/sprab37/sprab37.pdf.

[7] J. G. Webster. *Design of pulse oximeters*. Taylor and Francis Group, NY, 1997.

[8] V.S. Murthy, S. Ramamoorthy, N. Srinivasan, S. Rajagopal, and M.M. Rao. Analysis of photoplethysmographic signals of cardiovascular patients. In *Proc. IEEE EMBS Conf.*, page 2204 Ű 2207, Oct 2001.

[9] International Standard. *Medical electrical equipment - Particular requirements for the basic saftey and essential performance of pulse oximeter equipment for medical use*. ISO 9919:2005(E), Switzerland, 2005.

[10] D. Donoho. Compressed sensing. *IEEE Transactions on Information Theory*, 52:1289–1306, April 2006.

[11] E. Candes, J. Romberg, and T. Tao. Stable signal recovery from incomplete and inaccurate measurements. *Communications on Pure and Applied Mathematics*, 59:1207–1223, August 2006.

[12] M. A. T. Figueiredo, R. D. Nowak, and S. J. Wright. Gradient projection for sparse reconstruction: Applications to compressed sensing and other inverse problems. *IEEE Journal of Selected Topics in Signal Processing*, 1:586–598, Dec 2007.

[13] http://www.xilinx.com/support/documentation/.

[14] M. J. Hayes and P. R. Smith. Artifact reduction in photoplethysmography. *Applied Optics*, 37:7437–7446, November 1998.